The International Journal of Advanced Manufacturing Technology (2024) 131:3781–3792
https://doi.org/10.1007/s00170-024-13238-y

ORIGINAL ARTICLE

Optimization of shot peening parameters for blades based on the constraint of equivalent residual stress-induced deformation

Jiyin Zhang[1,2] · Changfeng Yao[1] · Weiwei Zhuo[2] · Liang Tan[1] · Minchao Cui[1] · Qing Wei[2]

Received: 11 December 2023 / Accepted: 10 February 2024 / Published online: 20 February 2024

Abstract

As a surface-strengthening technique, shot peening increases the compressive residual stress in the workpiece. In this paper, how to obtain specific residual stresses to reduce blade deformation by controlling the shot peening parameters was investigated. Based on the cosine function describing the residual stress depth distribution, the equivalent residual stress was calculated. The effect of shot peening parameters (air pressure, flow rate, nozzle speed, and distance) on the equivalent residual stress was modeled. Then a finite element model of the equivalent residual stress-induced deformation of the blade was established, and the effect of equivalent residual stress on blade deformation was investigated via the model. The residual stress domains that make the deformation less than 0.03 mm were obtained by the inverse solution of the exhaustive method, then the optimized parameter of shot peening was also obtained, and the accuracy of the optimization method was verified by shot peening tests. This method can provide technical support for the control of deformation caused by shot peening of blades.

Keywords Shot peening parameters · Equivalent residual stress · Blade · Deformation · Optimization

1 Introduction

During shot peening, the workpiece surface undergoes plastic deformation due to the impact of numerous high-speed projectiles. Internally, the material is subjected to stress that does not reach the yield strength and therefore, only elastic deformation occurs. When the projectile rebounds from the surface of the workpiece, there is a tendency for the interior to return to its original state, thus compressing the surface layer of the material, which causes residual compressive stress in the surface layer [1]. The compressive residual stress due to shot peening reduces the initiation of microcracks under fatigue stress and inhibits their early expansion, thus significantly improving the resistance to fatigue fracture and stress corrosion cracking of the workpiece [2–4]. For this reason, shot peening is widely used for aero-engine components [5].

The main mechanism of shot peening is the introduction of compressive residual stresses within the impact layer of shot peening [6]. The actual process of shot peening can be simulated by combining a discrete element method and finite element method. The predicted residual stress was verified with experimental measurements [7–9]. To overcome the limitations of traditional software in simulating the effects of shot peening, researchers have developed additional algorithms in MATLAB, Python, etc. [10–12]. For example, a numerical method in the Python programming language can simulate multiple projectiles using a random probability distribution [13]. Based on Hertzian contact theory[14], a modified theoretical model that considers the effect of friction between the projectile and the part can predict the residual stress field in aluminum–lithium alloys and other metallic materials under various shot peening conditions [15]. With the shot peening parameters as the input, artificial neural networks have been used to predict the residual stress due to shot peening [16–18]. An Almen intensity prediction model based on a model for the residual stress after shot

✉ Jiyin Zhang
zhangjiyin.chn@hotmail.com

✉ Changfeng Yao
chfyao@nwpu.edu.cn

✉ Weiwei Zhuo
zhuoweiwei826921@163.com

[1] Key Laboratory of High Performance Manufacturing for Aero Engine (Northwestern Polytechnical University), Ministry of Industry and Information Technology, Xi'an, Shaanxi 710072, People's Republic of China

[2] Chengdu State-Run Jinjiang Machinery Factory, Chengdu, Sichuan 610043, People's Republic of China

peening has been developed [19]. The results were in good agreement with experimental data. In addition, a white-box model developed in Python employs artificial neural networks to predict the residual stress caused by laser peening [20, 21]. This approach can also be applied to shot peening. A probabilistic approach has also been used to evaluate the residual stress distribution [22]. It can predict the residual stress profile after shot peening with a specific probability of occurrence. X-ray diffraction methods have been applied to determine the depth and magnitude of the macroscopic residual stress generated by shot peening [23, 24]. The stress distribution generated by a projectile impact has been approximated by cosine [25, 26] or sine curves [27] along the thickness direction in combination with a law for the depth of residual stress due to shot peening, as measured by saturation tests. A model for the residual stress based on Hertz contact theory has been proposed [28]. It considers the hardening properties of the material and the reverse yielding of the material around the crater. This model was used to calculate the stress components along the depth direction inside the target material below the impact point [29].

Optimization based on predicting the residual stress due to shot peening can be used to control the deformation caused by residual stress [30]. Two shot peening and application of pre-stress can optimize the distribution of compressive residual stresses and microstructure [31, 32]. In addition, multiple shot peening treatments contribute to the formation of high compressive residual stress layers [33]. The response surface method was used to evaluate the effect of process parameters on residual stresses, and based on this, the optimum shot peening parameters for maximum residual stresses were obtained [34]. Particle image velocimetry can accurately measure the projectile velocity for different air pressures [35], and a finite element model (FEM) for fine-particle shot peening has been developed based on this. The resulting predictions of the residual stress distribution obtained with a three-stage approach correlated well with the experimental data. Based on finite element simulation results, the maximum residual stress (MRS) and the depth of residual stress affected layer (DRSA) can be optimized using the response surface method [36].

The prediction of deformation induced by residual stress forms the basis for controlling deformation. There are three main simulation methods for shot peening: equivalent heat load method [37, 38], in-face extrusion method [39], and direct stress method [30]. The surface residual stress field is mathematically analyzed and is equivalent to a set of face and edge loads. The part deformation problem is equivalent to an elastic deformation problem and is solved by finite element software. The method is considered particularly suitable for large curved parts, such as propellers and blades [40]. The processing of thin-walled parts is a rather complex process, and there are more factors to be considered. Based on the finite element simulation, the blade back and blade basin are strengthened by different shot peening intensities, which can well reduce the deformation of the large fan blade after shot peening [41]. Prestress shot peening is used to correct deformed structural members with asymmetric cross sections [42]. The different machining positions will cause different workpiece deformations. Based on the finite element analysis, the shot peening forming area and parameters were designed for the AA7050 integral reinforcement plate, and the test results of external torsional curvature met the requirements of the aircraft airfoil [43]. Based on an idealized model of the shot peening process, an optimization procedure is established to automatically calculate the shot peening pattern so that the deformation after shot peening is the desired target shape [44]. Active control fixtures for blade parts are employed to adjust deformation during machining by balancing internal stresses and preventing redistribution of residual stresses after the final machining step [45]. Six-peak Gaussian function was introduced to fit the initial residual stress, a deformation prediction model between initial residual stress and finishing allowance was established, and linear programming optimization model based on the simplex algorithm was developed to optimize the overall machining deformation[46].

Most of the studies aimed at the residual stresses and their deformation due to shot peening have focused on the effect of shot peening parameters on the residual stresses, and based on this, their deformation is studied. In this paper, the equivalent residual stress (ERS) was used to describe the residual stresses caused by shot peening. Then, the relations for the effects of shot peening parameters on the ERS were obtained. Based on this, the effect of ERS on blade deformation were studied, and finally the optimized parameters of shot peening to meet the deformation requirements was obtained by the inverse solution of the exhaustive method. This has positive implications for quantifying the residual stresses caused by shot peening and optimizing residual stress-induced deformation.

2 Equivalent residual stress of shot peening

The depth distribution of the residual stress due to shot peening is mostly described by fitting a curve. In this section, a cosine function was used to describe the distribution of residual stress along the depth, the surface residual stress (SRS), the MRS, the depth of maximum residual stress (DMRS), and DRSA, which characterize the residual stress, were obtained from derivative and inverse functions. Combining the DRSA and the cosine function for the residual stress, the ERS, which also characterizes the residual stress, was obtained by integration. Finally, the relation for the

effects of shot peening parameters on residual stress was obtained.

2.1 Characterization of equivalent residual stress

2.1.1 Characteristic parameters of residual stress

Various functions are commonly used to describe the depth distribution of the residual stress due to shot peening, with the cosine function being one of the most widely used:

$$\sigma(h) = Ae^{\lambda h}\cos(\omega h + \theta) + D \tag{1}$$

where σ is the residual stress, h is the depth beneath the surface, and A is the amplitude of the underdamped oscillation. λ is a damping coefficient, which determines how quickly the profile will settle to a steady value. ω is the damped frequency. It is proportional to the inverse of the period of the profile. For higher ω, the period of the profile is shorter, giving a sharper peak to the SRS. θ is the phase angle. It is in the range $[-\pi, +\pi]$. D is an offset parameter used to match the regression formula to the measured residual stress profile.

From Eq. (1), we get

$$\sigma\prime(h) = A\lambda e^{\lambda h} \times \cos(\omega h + \theta) - A\omega e^{\lambda h}\sin(\omega h + \theta)) \tag{2}$$

Let $f(x)$ be the inverse function of Eq. (1) and $g(x)$ be the inverse function of Eq. (2). The characteristic parameters of the residual stress field can easily be calculated in Python or by other software as follows: SRS $\sigma_{surface} = \sigma(0)$, MRS $\sigma_{max} = \sigma(g(0))$, DMRS $H_{max} = g(0)$, and DRSA $H = f(0)$. These are plotted in Fig. 1.

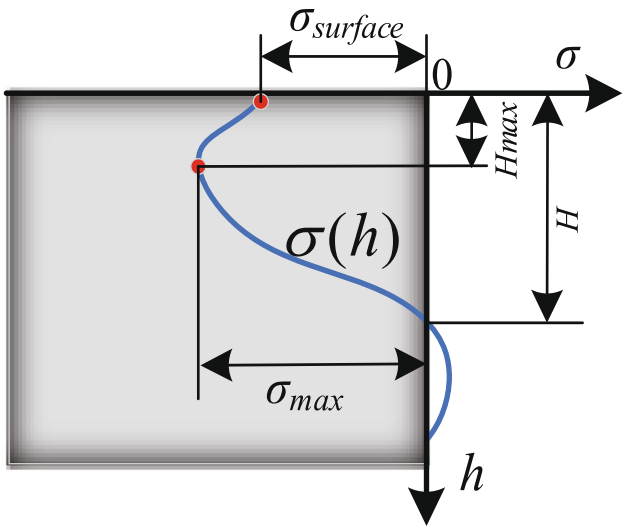

Fig. 1 Characteristic value of residual stress: $\sigma_{surface}$ is the surface residual stress, σ_{max} is the maximum residual stress, H_{max} is the depth of maximum residual stress, and H is the depth of residual stress affected layer

2.1.2 Equivalent residual stress

The depth distribution of the residual stress is mostly characterized by fitting data points. The SRS, MRS, DMRS, and DRSA can then be calculated as in the previous section to describe the residual stress quantitatively. However, these four values are complex, and it is difficult to quantify their relations with deformation. Thus, they are not conducive to compare the residual stress distribution for the multiple sets of parameter values. Therefore, in this section, we combine the characteristic parameter H from the residual stress depth shown in Fig. 1 with the residual stress depth of Eq. (1) to give the ERS.

The equivalent method is based on the "equal moment" principle. The method is as follows: (a) The measured residual stress data in the depth direction are interpolated and fitted to obtain the residual stress depth distribution curve σ(h) shown in Fig. 1, where h is the depth under the surface. (b) The stress σ is the internal force per unit area, that is,

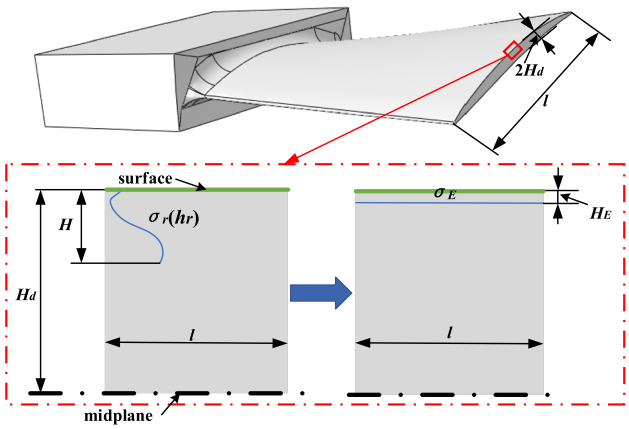

Fig. 2 Equivalent residual stress: Hd is the distance from its surface to the midplane, H is the depth of residual stress affected layer, $\sigma(h)$ is the residual stress depth distribution curve, l is the width of thin-plate specimen, σ_E is the ERS, and H_E is the influence layer depth of ERS

$\sigma = F/\Delta S$, combined with Fig. 2, assuming that the width of thin-plate specimen is l, we can see that

$$\sigma(h) = \frac{F}{l \times \Delta h} \tag{3}$$

$$F = \sigma(h) \times l \times \Delta h \tag{4}$$

(c) Let the thickness of the blade be $2H_d$ and the distance from its surface to the midplane be H_d. The moment of the residual stress affecting layer can be expressed as

$$M = \int_{H_d}^{H_d-H} (F \times h)dh = \int_{H_d}^{H-H} (\sigma(h) \times l \times (H-h) \times h)dh \tag{5}$$

(d) Let the ERS be a constant value σ_E, depth is H_E, then

$$M_E = \int_{H_d}^{H_d-H_E} (\sigma_E \times l \times h)dh \tag{6}$$

(e) By the principle of equal moments, $M = M_E$, then

$$\int_{H_d}^{H_d-H} (\sigma(H-h) \times l \times h)dh = \int_{H_d}^{H_d-H_E} (\sigma_E \times l \times h)dh \tag{7}$$

and l is a constant, then

$$\int_{H_d}^{H_d-H} (\sigma(H-h) \times h)dh = \int_{H_d}^{H_d-H_E} (\sigma_E \times h)dh \tag{8}$$

(f) Therefore, the ERS is

$$\sigma_E = \frac{\int_{H_d}^{H_d-H} (\sigma(H-h) \times h)dh}{\int_{H_d}^{H_d-H_E} hdh} \tag{9}$$

By substituting H_d, H, H_E, and $\sigma(h)$ in function (8), the ERS value σ_E can be obtained. The residual stress can be characterized by ERS and its influence layer depth of H_E.

Table 1 Material property parameters of titanium alloy TC17

Categories	Parameter	Value
Basic constants	Density ρ (kg/m^3)	4770
	Young's modulus E (GPa)	112
	Poisson's ratio	0.34
Constants of J–C model	Melting temperature T_{melt} (K)	1675
	Initial yield stress A (MPa)	1100
	Hardening constant B (MPa)	700
	Hardening exponent n	0.983
	Strain rate constant C	0.01
	Thermal softening exponent m	0.7

2.2 Equivalent residual stresses of TC17 titanium alloy

2.2.1 Measurement of residual stress

The TC17 titanium alloy was used in this study (Ti–5Al–2Sn–2Zr–4Mo–4Cr). It was heat treated at 360 °C for 30 min and 550 °C for 3–4 h before being allowed to cool in air. Its chemical composition was 4.5–5.5% Al, 1.6–2.4% Sn, 1.6–2.4% Zr, 3.5–4.5% Mo, 3.5–4.5% Cr, and Ti balance 21%. The mechanical properties are listed in Table 1, and a specimen is shown in Fig. 3(a).

Three points were selected for measuring the residual stress of each specimen, as shown in Fig. 3(b). The residual stress was measured in the x and y directions, to give the average values of the residual stress in the x and y directions, which were used for the subsequent analyses.

Of the several techniques available for measuring the residual stress, X-ray diffraction was utilized in this study. The residual stress was measured on a residual stress measuring system (LXRD MG2000, PROTO), as shown in Fig. 4(a). Taking material properties and equipment performance into consideration, the parameters for measuring the residual stress of TC17 were selected, as shown in Table 2.

First, a measurement point was electropolished with a saturated solution of CH_3OH, $C_6H_{14}O_2$, and $HClO_4$ in the ratio 10:5:1 to expose the deeper layers. The workpiece was etched several times in a direction perpendicular to the surface using an electrolytic polisher, as shown in Fig. 4(b). The subsurface residual stress in each layer was measured after each etching cycle. Measured data on residual stress do exhibit errors. However, the values were only about ± 20 MPa, and therefore, they will be ignored in the following analysis and simulation.

2.2.2 Characterization model for equivalent residual stresses of TC17 titanium alloy

Based on the shot peening parameters of the blade, the test was planned using the response surface method with air pressure, flow rate, nozzle speed, and distance as variables for the

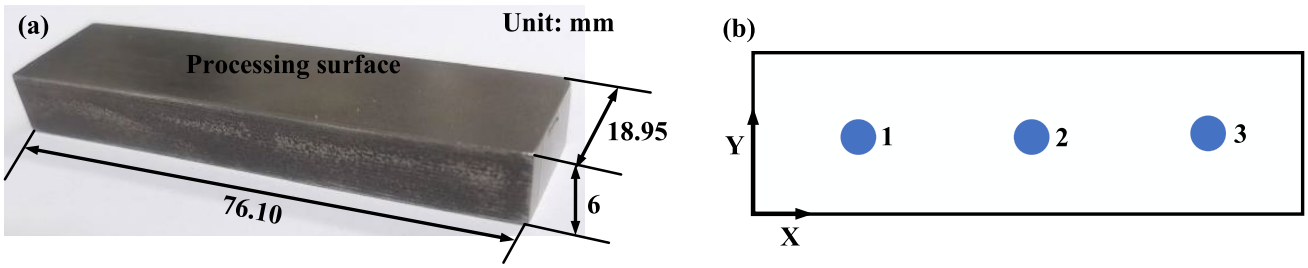

Fig. 3 Specimen and measurement points: **a** block specimen; **b** planning for measuring residual stress, three measurement points are evenly distributed on the machined surface

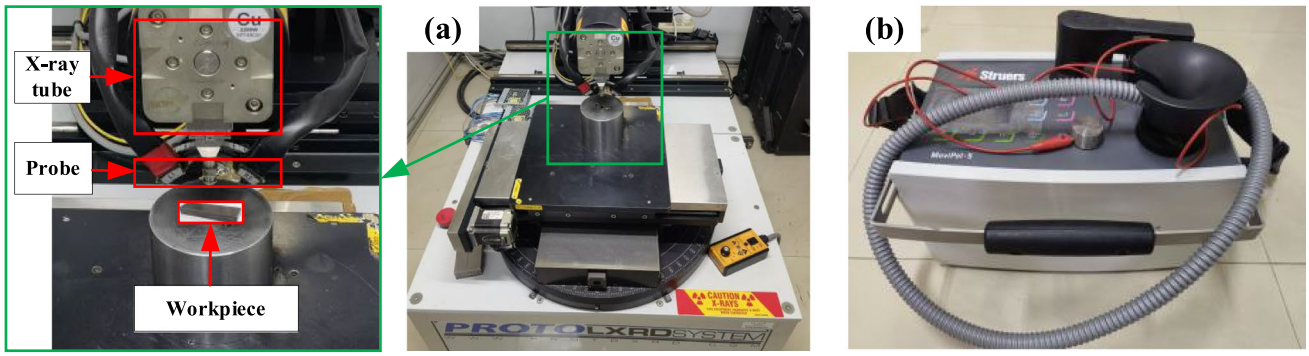

Fig. 4 Residual stress measurement system and electrolytic polisher: **a** PROTO-LXRD MG2000 residual stress measuring system; **b** Struers MoviPol-5 electrolytic polisher

Table 2 Parameters for measuring the residual stress of TC17 alloy

Category	Parameter	Value
Measurement constants	Voltage (kV)	25
	Current (mA)	20
	X-ray tube	Cu_Kα
	β angle	$\pm 25°$
	Diffraction crystal plane	{213}
	Bragg angle 2θ	142°
	Number of exposures	10
	Exposure time (s)	2
	Collimator diameter (mm)	3
Elastic constants	$\nu^{\{213\}}$	0.32
	$\frac{1}{2}S_2^{\{213\}}$(mm^2/N)	12.0×10^{-6}
	$S_1^{\{213\}}$(mm^2/N)	-2.9×10^{-6}

specimen shown in Fig. 3(a). The experimental protocol is shown in Table 3.

Next, we analyze the results for different parameter sets. Combined with the calculation method of characteristic parameters and ERS in Sect. 2.1, the characterization of residual stresses for 29 sets of shot peening parameters in Table 3 is shown in Table 4.

Table 4 shows that the SRS, MRS, DMRS, DRSA, and ERS depend on the shot peening parameters. The ERS is clearly different for the different sets. Thus, we have demonstrated that the ERS can be used to characterize the residual stress-affected layer. Further the ERS can be used in a mathematical relation between the residual stress-affected layer and fatigue or deformation.

2.3 Effects of shot peening parameters on equivalent residual stress for TC17 titanium alloy

According to the characterization amount of shot peening parameters corresponding to each group of shot peening

Table 3 Experimental planning of response surface method based on shot peening parameters

Set	Air pressure (MPa)	Flow rate (kg/min)	Nozzle speed (mm/min)	Distance (mm)
1	0.1	0.95	60	25
2	0.1	0.8	30	25
3	0.1	0.8	60	15
4	0.1	0.6	60	25
5	0.15	0.95	60	15
6	0.1	0.6	60	5
7	0.06	0.6	60	15
8	0.1	0.8	60	15
9	0.15	0.8	120	15
10	0.1	0.95	30	15
11	0.15	0.8	60	25
12	0.06	0.95	60	15
13	0.1	0.6	120	15
14	0.1	0.8	60	15
15	0.06	0.8	30	15
16	0.1	0.8	120	5
17	0.1	0.8	30	5
18	0.06	0.8	120	15
19	0.06	0.8	60	25
20	0.15	0.8	30	15
21	0.1	0.6	30	15
22	0.1	0.8	60	15
23	0.1	0.95	60	5
24	0.1	0.8	60	15
25	0.06	0.8	60	5
26	0.15	0.8	60	5
27	0.1	0.8	120	25
28	0.15	0.6	60	15
29	0.1	0.95	120	15

parameters as shown in Table 4, regression analysis was performed to finally obtain the characterization model of residual stress based on air pressure, flow rate, moving speed and distance, as shown in Eqs. (10) and (11), with adjusted R squared is greater than 0.95, indicating a high accuracy of the model.

$$\begin{aligned} DRSA &= 191.08334 + 78.92062 * p - 354.76632 * q - 0.64687 * v - 1.06297 * h \\ &+56.33945 * p * q - 0.150859 * p * v - 0.2024 * p * h - 0.08232 * q * v \\ &+0.304672 * q * h + 0.001381 * v * h - 32.5728 * p^2 + 192.1611 * q^2 \\ &+0.003804 * v^2 + 0.027237 * h^2 \end{aligned} \tag{10}$$

$$\begin{aligned} ERS &= -671.71518 + 99.55008 * p - 247.88998 * q + 2.42216 * v + 2.27525 * h \\ &-181.03826 * p * q + 2.449518 * p * v + 2.263936 * p * h + 0.307665 * q * v \\ &-1.38011 * q * h - 0.00540 * v * h - 60.51072 * p^2 + 196.57537 * q^2 \\ &-0.024536 * v^2 - 0.081603 * h^2 \end{aligned} \tag{11}$$

Table 4 Characterization of residual stresses for different shot peening parameters

Set	SRS (MPa)	MRS (MPa)	DMRS (mm)	DRSA (mm)	ERS (MPa)
1	−785.8	−832.85	0.01334	0.06434	−622.29
2	−889.02	−927.84	0.01567	0.0756	−683.26
3	−757.52	−808.17	0.01627	0.07965	−602.97
4	−734.58	−775.38	0.0174	0.0978	−570.26
5	−819.76	−840.19	0.02002	0.09217	−618.45
6	−756.19	−797.46	0.01178	0.05377	−590.84
7	−738.2	−794.16	0.01424	0.07229	−594.52
8	−757.52	−808.17	0.01567	0.0756	−602.97
9	−687	−716.19	0.01364	0.06037	−526.04
10	−966.87	−995.81	0.01342	0.0675	−702.55
11	−773.8	−801.79	0.0183	0.09592	−601.91
12	−748.76	−886.97	0.01042	0.0489	−644.68
13	−707.12	−747.23	0.012	0.05377	−545.22
14	−757.52	−808.17	0.0177	0.10522	−602.97
15	−763.79	−819.64	0.0216	0.099	−635.49
16	−721.84	−769.55	0.01567	0.0756	−565.5
17	−931.31	−964.83	0.01837	0.087	−691.43
18	−771.7	−840.51	0.01567	0.0756	−639.56
19	−752.37	−821.26	0.01222	0.05445	−637.94
20	−1052.94	−1068.13	0.02122	0.09652	−754.34
21	−876.94	−914.79	0.01342	0.06742	−688.31
22	−757.52	−808.17	0.01815	0.09157	−602.97
23	−804.19	−850.46	0.01365	0.06862	−633.81
24	−757.52	−808.17	0.01334	0.06434	−602.97
25	−750.78	−819.44	0.01567	0.0756	−637.69
26	−826.74	−853.21	0.01627	0.07965	−641.49
27	−721.44	−769.21	0.0174	0.0978	−562.89
28	−714.31	−735.13	0.02002	0.09217	−527.05
29	−722.58	−769.74	0.01178	0.05377	−563.13

3 FEM of equivalent residual stress-induced deformation

In this part, the equivalent residual stresses were loaded on the blade model according to the actual processing condition of shot peening, the FEM of equivalent residual stress-induced deformation was established, and the deformation was studied.

3.1 Blades and their machining process

3.1.1 Characteristics of the blade profile

The model of the blade in this study is a semi-finished workpiece; as shown in Fig. 5, its profile part is consistent with that of the actual blade, whose dimensions are roughly 100 mm × 70 mm, while the blade root part, which is not related to deformation, is a roughly machined square. The outer contour of the fan blade is composed of three-dimensional free surfaces. The curvature radius of the blade tip is much larger than the root. The curvature radius is generally reduced from the tip region to the root region.

3.1.2 Machining of blade

The material of blade is TC17 titanium alloy, and after the blade was milled from blank, it was polished, and then shot peening, and the blade will be polished again if the surface roughness is not satisfactory. This paper mainly studies the residual stress-induced deformations of blade after shot peening. The shot peening was finished on the MP1500TX shot peening machine of Wheelabrator company.

3.2 Equivalent residual stresses loaded in the blade

In the shot peening process of blade, the impact range of the shot is much smaller than the blade surface area, so it

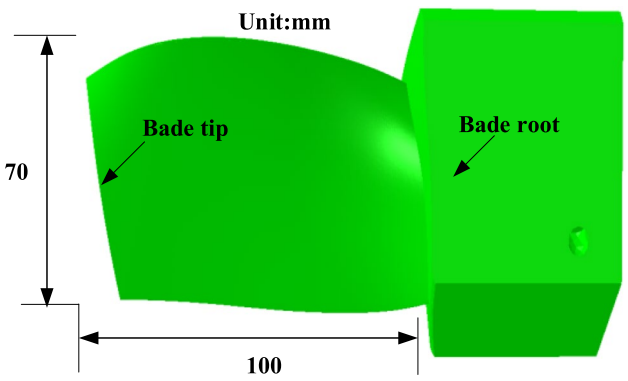

Fig. 5 Compressor blade

is impossible to complete full coverage at one time, need to plan a good shot peening trajectory, so that the nozzle along the planned trajectory to move, to ensure that the entire blade surface is covered by the projectiles.

As shown in Fig. 6, the nozzle was walking back and forth three times during the shot peening process to ensure that the coverage was as required. To make the FEM of shot peening closer to the real situation, and considering the time required for the FEM, the blade surface was divided into nine regions as much as possible according to the equal area principle, and residual stresses were applied in each region in turn to simulate the actual shot peening process. This makes the loaded residual stresses close to the actual residual stresses on the workpiece, thus ensuring the accuracy of the finite element analysis.

The residual stresses loaded in the FEM are obtained based on the ERS calculation method in Sect. 2.1. Based on the measured residual stress data, the ERS and their affected layer depths are calculated for the specific shot peening parameters.

The process of loading ERS based on the time sequence is shown in Fig. 6. Take the shot peening process of blade back as an example, choose the shot path "the nozzle carries out horizontal movement, starting from the blade root and ending at the blade tip." The calculated ERS is loaded into the *Bk1* region, and the results including the blade deformation and stress state are obtained after finite element analysis; then the result file is imported into Abaqus software as the initial state of the model, and then the ERS is loaded in the *Bk2* region of this model for finite element analysis, and the result file is obtained; again the result file is imported into the software, and the ERS is applied in the *Bk3* region, and so on, loading ERS in each region in the planned order to simulate the actual shot peening process.

3.3 Finite element analysis of residual stress-induced deformation

The geometric model of the blade is imported into Abaqus software, and the coordinate system in Abaqus software is the same as the design coordinate system of the blade. The shell is extracted from the blade back and the blade basin, and the shell thickness is set to the same depth as the influence layer of ERS. The shell is divided into nine regions as uniformly as possible, and then the shell and the blade are bound together by the "tie" method.

The material properties of TC17 are entered in the "properties" module. The thickness of the shell is set according to the DRSA. The analysis of the blade deformation is based on the blade root, so the blade root model is constrained when establishing the boundary conditions. The six degrees of freedom of the blade root are fully constrained.

The mesh size is closely related to the analysis time and the accuracy of FEA results. Too large mesh size has low analysis accuracy, and too small mesh size will prolong the analysis time. After several experiments and explorations, a meshing method that considers both analysis accuracy and time cost is adopted. The cell size of the blade surface part is 0.5 mm, the cell size of the root part is 1 mm, the cell type is C3D10, and the total number of cells is 269,264. The cell size of the blade shell is 0.5 mm, the cell type is S4R, and the total number of cells is 12,714.

The TC17 blade was subjected to residual stress-induced deformation simulation, and the ERS and the DRSA corresponding to the 15 and 21 groups of parameters in Table 3 were selected. The finite element analysis results of the blade are shown in Fig. 7, and it can be found that the deformation

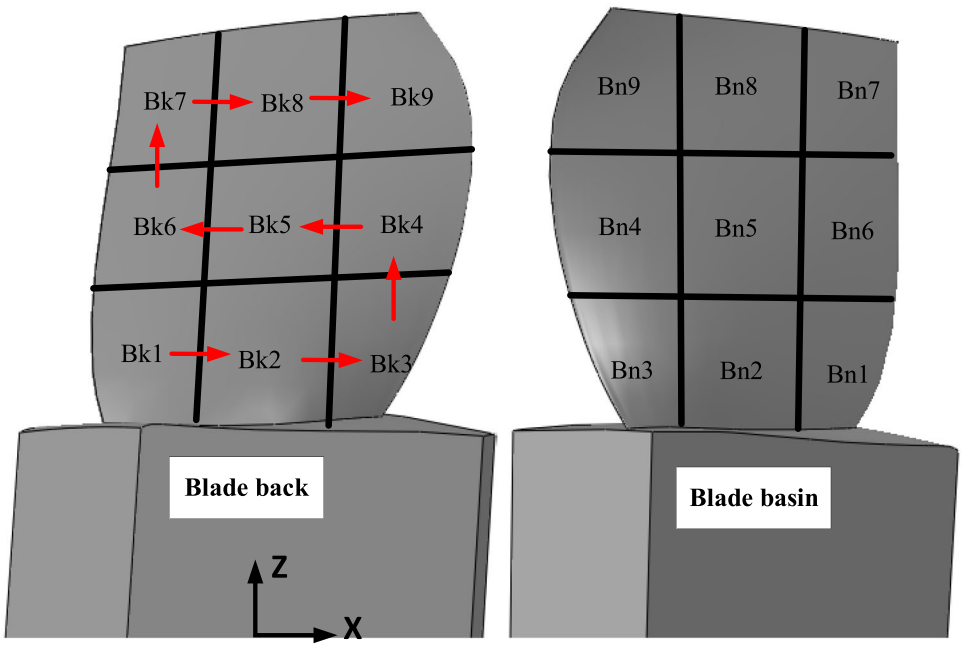

Fig. 6 Time sequence of blade shot peening: ERS are loaded sequentially in the order shown by the red arrows

decreases gradually from the blade tip to the blade root, so the deformation at the blade tip is selected for subsequent analysis.

In the blade design model, the inlet side to the exhaust side is set as x-direction and the blade basin to the blade back as y-direction. The simulated deformation of group 15 and group 21 is compared with its measured results; the results are shown in Fig. 8. The analysis found that the x-direction deformations of group 15 and group 21 are relatively small compared with the y-direction. Comparing the measured deformation and simulated deformation, the difference between the x-direction deformation is not large, and the maximum difference between the y-direction deformation is 20%, but the trend is consistent, so the FEM can be used for further study of the residual stress-induced deformation of TC17 blade.

4 Optimization of shot peening parameters based on deformation constraints

Based on the FEM of equivalent residual stress-induced deformation, the effect of shot peening parameters on deformation was obtained, and the optimized shot peening parameters were obtained by exhaustive haircut calculation. Finally, the optimized shot peening parameter was verified.

4.1 Residual stress control domain based on deformation constraints

To analyze the influence relationship between the ERS and DRSA on the deformation of TC17 blade, finite element analysis is performed with the verified FEM of residual stress-induced deformation for each group of shot peening parameters in Table 3 to obtain the deformation of the blade under each group of ERS and DRSA conditions. The influence relationship model is shown in Eqs. (12) and (13). Figure 9 depicts the influence relationship between them; it can be found that the deformations in both x-direction and y-direction decrease with the decrease of the ERS and DRSA.

$$Ux = 0.00361 + 5.245e^{-6} * ERS - 0.0521 * hr + 2.0204e^{-4} * ERS * hr - 2.967e^{-8} * ERS^2 * hr + 3.346e^{-5} * ERS * hr^2 + 2.369e^{-9} * ERS^2 + 0.225 * hr^2 \quad (12)$$

$$Uy = -0.022 + 8.985e^{-5} * ERS + 1.797 * hr + 0.0017 * ERS * hr - 2.807e^{-6} * ERS^2 * hr - 0.0270 * ERS * hr^2 + 2.183e^{-7} * ERS^2 - 17.525 * hr^2 \quad (13)$$

where ERS is the equivalent residual stress and hr is the depth of the residual stress-affected layer.

According to the relationship between the ERS and DRSA on the deformation, the ERS and DRSA control domains based on the deformation constraint are inverse solved by the exhaustive method. According to Table 4, the range of the ERS is $[-526.04, -754.34]$ and the range of the DRSA is [0.049, 0.105]. Since a large compressive residual stress and its influence layer depth can improve the fatigue life of the blade [47], this optimization is bounded by the median value of ERS and DRSA; that is, the initial domain is set as follows:

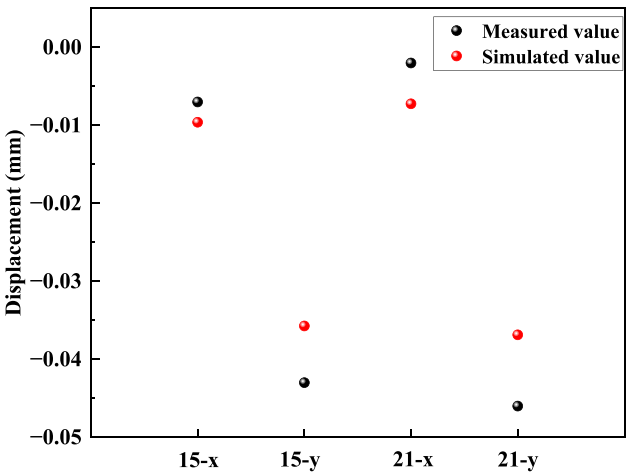

Fig. 8 Verification of FEM for residual stress-induced deformation: set 15 and set 21 in Table 2

Fig. 7 Finite element analysis results of residual stress-induced deformation: take normal deformation as an example

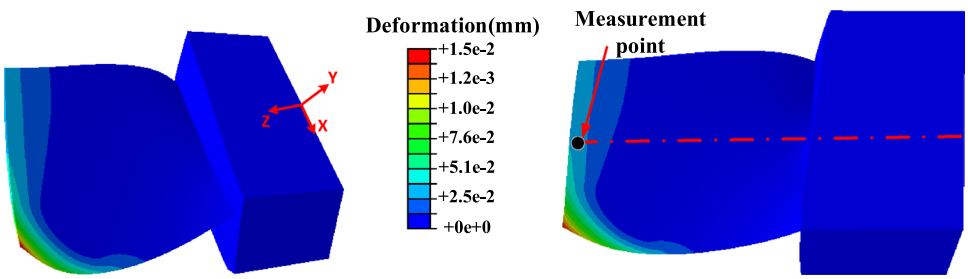

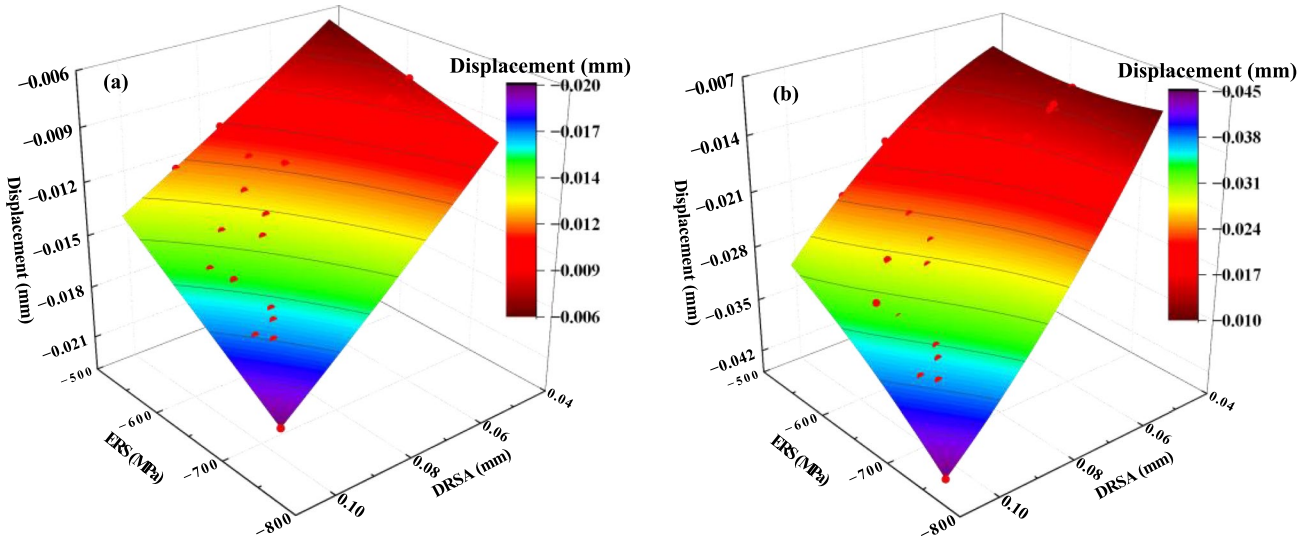

Fig. 9 Effect of ERS and DRSA on the deformation of TC17 blade: **a** displacement in the *x*-direction; **b** displacement in the *y*-direction. ERS indicates the equivalent residual stress; DRSA indicates the depth of residual stress affect layer

ERS [−640.19, −754.34], DRSA [0.077, 0.105], and the constraint is set as the absolute value of deformation < 0.03 mm. From Table 2, the resolution of the ERS and DRSA can be set to 5 MPa and 0.005 mm. A program is written in Python to perform the calculation and generate two sets of equal difference series LDRSA and LERS based on the initial domain of each parameter. The two nested loops are prepared, and a value is extracted from the two initial domains in order to arrange the combinations, and the combinations are assigned to Eq. (12), if the calculation result of Ux is within the range of [−0.03, 0.0], then the parameter combinations are adopted and broken up into two new series LXDRSA and LXERS, respectively, and discarded if they are out of range. Two parameter series that meet the *x*-direction deformation constraint are obtained. Subsequently, two nested loops are prepared again, and a value is extracted from the two new series LYDRSA and LYERS in order to arrange the combination, and each combination is assigned to Eq. (13), if the result of ERS calculation within the range of [−0.03, 0.0] is used and the combination of parameters is broken into two new series LUDRSA and LUERS, respectively, and discarded if it is out of range. Finally, the two series are derived and processed to obtain a combination of residual stress that meet the requirements, as shown in Table 5, and the comprehensive analysis finds that the specific control domains are ERS [−664, −754] and DRSA [0.077, 0.082].

4.2 Shot peening parameters based on deformation constraints

The distance between the nozzle and the blade in the shot peening process is always varying between 5 and 25 mm, so the distance *h* is set to 15 mm in this study. The combinatorial enumeration in the exhaustive method is used in this part, i.e., the values are taken in the range of air pressure, flow rate, and nozzle speed, and they are combined with each other arbitrarily to try whether they satisfy the constraints of the ERS and DRSA.

Based on Table 3, the initial domains of the shot peening control parameters were set, i.e., air pressure *p*[0.6,1.5], flow

Table 5 Control domain of ERS and DRSA based on deformation constraint

Set	ERS (MPa)	DRSA (mm)
1	−754	0.077
2	−749	0.077
3	−744	0.077
4	−739	0.077
5	−734	0.077
6	−729	0.077
7	−724	0.077
8	−719	0.077
9	−714	0.077
10	−709	0.077
11	−704	0.077
12	−704	0.082
13	−699	0.077
14	−699	0.082
15	−694	0.077
……	……	……
39	−644	0.077
40	−644	0.082

rate q[0.6,0.95], and nozzle speed v[30,120]. Due to the control accuracy of air pressure and flow rate in the shot peening process is 0.05, so the domain resolution of air pressure and flow rate is set to 0.05, and the domain resolution of nozzle speed is set to 10 due to the small differentiation. Combined with Eqs. (10) and (11), a program was written in Python to perform the calculations and obtain the combination of shot peening control parameters that meet the requirements, as shown in Table 6.

Given the wide range of parameters obtained, further determination of the exact parameters is required. Combined with Eqs. (10) and (11), the ERS corresponding to each group of parameters in Table 6 is calculated here, and its DRSA is set to 0.08 mm for the purpose of analysis. Since a large compressive residual stress and its influence layer depth can improve the fatigue life of the blade [47], the first group is selected as the optimal shot peening parameters after comparative analysis.

4.3 Shot peening processing of blade

Optimized shot peening parameters for the TC17 blade required shot peening tests to verify its feasibility. The blade was shot peened using the MP1500TX shot peening machine from Wheelabrator company.

After the blade shot peening process is completed, the clamping is removed and left for a period of natural aging, the deformation is measured on a CMM with the tenon root as the reference and the design model coordinate system as the measurement coordinate system according to the process drawing. The deformation results are shown in Fig. 10.

Figure 10 compares the processing deformation of each of the three blades processed with the original shot peening parameters and optimized shot peening parameters, and the deformation of each blade is the deformation of the measurement point. Though the comparative analysis found that the use of the original shot peening parameters of the blade after processing the x-direction and y-direction deformation are relatively large, the largest is located in the tip of the leaf, its deformation is 0.07 mm; using the optimized shot peening parameters for shot peening processing, their deformations are reduced, each section of the x- and y-direction deformations are reduced to within 0.02 mm, and the deformation of each section becomes more uniform compared to the other, which proves the feasibility of optimizing the shot peening processing parameters.

Table 6 Domains of air pressure, flow rate, nozzle speed, and distance that satisfy the deformation constraint

Set	Air pressure (MPa)	Flow rate (kg/min)	Nozzle speed (mm/min)	Distance (mm)	ERS (MPa)
1	0.07	0.6	30	15	700.92
2	0.08	0.7	30	15	666.71
3	0.08	0.8	30	15	617.71
4	0.08	0.9	30	15	621.88
5	0.08	0.6	40	15	666.72
6	0.09	0.7	40	15	660.88
7	0.09	0.8	40	15	639.78
8	0.09	0.9	40	15	665.60

5 Conclusions

This paper studied the residual stress-induced deformation of TC17 titanium alloy due to shot peening.

(1) Based on the cosine function for the residual stress for different sets of shot peening parameters, the ERS of shot peening residual stress was calculated using integration. Then the relation for the effects of shot peening parameters on residual stress was obtained.
(2) The equivalent residual stresses were loaded on the blade model according to the actual processing condition of shot peening; the FEM with high accuracy of equivalent residual stress-induced deformation was established.
(3) Based on the FEM, the effects of shot peening parameters on blade deformation were studied, and the optimized parameters of shot peening to meet the deformation requirements were obtained by the exhaustive method. This approach may serve as a new research tool and provide new ideas for studying the residual stress after shot peening as well as the control of deformation.

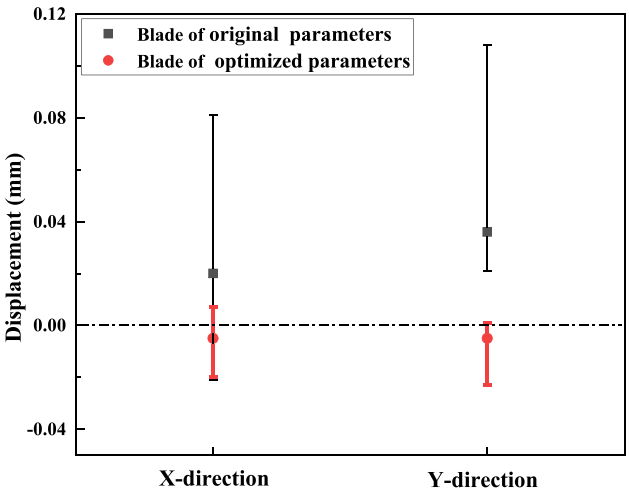

Fig. 10 Deformation of three blades machined using original shot peening parameters and optimized parameters, respectively. Measurement point of deformation amount is as shown in Fig. 7. The positive x-direction is taken from intake side to exhaust side and the positive y-direction from blade back to blade basin

Author contribution All authors contributed to the study conception and design. Conceptualization, methodology, and writing—original draft preparation were performed by Jiyin Zhang. Resources, funding acquisition, and supervision were performed by Changfeng Yao. Methodology and supervision were performed by Weiwei Zhuo. Data curation and writing—reviewing and editing were performed by Liang Tan. Methodology and project administration were performed by Minchao Cui. Investigation was performed by Qing Wei. And all authors commented on previous versions of the manuscript. All authors read and approved the final manuscript.

Funding This work was supported by National Natural Science Foundation of China (grant numbers 51875472, 91860206, 51905440, and 92160301), National Science and Technology Major Project (grant number 2017-VII-0001–0094), Key Research and Development Program of Shaanxi Province (grant number 2021ZDLGY10-06), and China Postdoctoral Science Foundation (grant number 2022M712199).

Data availability Not applicable.

Code availability Not applicable.

Declarations

Ethics approval Not applicable.

Consent to participate Not applicable.

Consent for publication Not applicable.

Competing interests The authors declare no competing interests.

References

1. Soady KA (2013) Life assessment methodologies incoroporating shot peening process effects: mechanistic consideration of residual stresses and strain hardening Part 1 – effect of shot peening on fatigue resistance. Mater Sci Technol 29:637–651. https://doi.org/10.1179/1743284713Y.0000000222
2. Thompson SR, Ruschau JJ, Nicholas T (2001) Influence of residual stresses on high cycle fatigue strength of Ti–6Al–4V subjected to foreign object damage. Int J Fatigue 23:405–412. https://doi.org/10.1016/S0142-1123(01)00166-9
3. Sharman ARC, Aspinwall DK, Dewes RC, Clifton D, Bowen P (2001) The effects of machined workpiece surface integrity on the fatigue life of γ-titanium aluminide. Int J Mach Tools Manuf 41:1681–1685. https://doi.org/10.1016/S0890-6955(01)00034-7
4. Wang C, Lai Y, Wang L, Wang C (2020) Dislocation-based study on the influences of shot peening on fatigue resistance. Surf Coat Technol 383:125247. https://doi.org/10.1016/j.surfcoat.2019.125247
5. Ramakokovhu U, Desai D, Snedden G, Jamiru T (2021) Significance of residual stresses in fatigue life prediction of micro gas turbine blades. Eng Fail Anal 120:105092. https://doi.org/10.1016/j.engfailanal.2020.105092
6. Kobayashi M, Matsui T, Murakami Y (1998) Mechanism of creation of compressive residual stress by shot peening. Int J Fatigue 20:351–357. https://doi.org/10.1016/S0142-1123(98)00002-4
7. Murugaratnam K, Utili S, Petrinic N (2015) A combined DEM–FEM numerical method for shot peening parameter optimisation. Adv Eng Softw 79:13–26. https://doi.org/10.1016/j.advengsoft.2014.09.001
8. Tu F, Delbergue D, Miao H et al (2017) A sequential DEM-FEM coupling method for shot peening simulation. Surf Coat Technol 319:200–212. https://doi.org/10.1016/j.surfcoat.2017.03.035
9. Li K, Wang C, Hu X et al (2021) DEM-FEM coupling simulation of residual stresses and surface roughness induced by shot peening of TC4 titanium alloy. Int J Adv Manuf Technol. https://doi.org/10.1007/s00170-021-07905-7
10. Qiang B, Li Y, Yao C, Wang X (2018) Effect of shot peening coverage on residual stress field and surface roughness. Surf Eng 34:938–945. https://doi.org/10.1080/02670844.2017.1391939
11. Pham TQ, Khun NW, Butler DL (2017) New approach to estimate coverage parameter in 3D FEM shot peening simulation. Surf Eng 33:687–695. https://doi.org/10.1080/02670844.2016.1274536
12. Lin Q, Liu H, Zhu C, Parker RG (2019) Investigation on the effect of shot peening coverage on the surface integrity. Appl Surf Sci 489:66–72. https://doi.org/10.1016/j.apsusc.2019.05.281
13. Zhou F, Jiang W, Du Y, Xiao C (2019) A comprehensive numerical approach for analyzing the residual stresses in AISI 301LN stainless steel induced by shot peening. Materials (Basel) 12:3338. https://doi.org/10.3390/ma12203338
14. Sherafatnia K, Farrahi GH, Mahmoudi AH (2018) Effect of initial surface treatment on shot peening residual stress field: analytical approach with experimental verification. Int J Mech Sci 137:171–181. https://doi.org/10.1016/j.ijmecsci.2018.01.022
15. Gao Y, Tao X (2020) Investigation on theoretical analysis of residual stress distribution induced by shot peening in 2397 aluminum-lithium alloy. In advanced surface enhancement: proceedings of the 1st International Conference on Advanced Surface Enhancement (INCASE 2019)—research towards industrialisation. Springer, Singapore, pp 56–68. https://doi.org/10.1007/978-981-15-0054-1_7
16. Maleki E, Farrahi GH, Sherafatnia K (2016) Application of artificial neural network to predict the effects of severe shot peening on properties of low carbon steel. In: Öchsner A, Altenbach H (eds) Machining, joining and modifications of advanced materials. Springer, Singapore, pp 45–60
17. Shen X, Shukla P, Subramaniyan AK, Zammit A, Swanson P, Lawrence J, Fitzpatrick ME (2020) Residual stresses induced by laser shock peening in orthopaedic Ti-6Al-7Nb alloy. Opt Laser Technol 131:106446. https://doi.org/10.1016/j.optlastec.2020.106446
18. Mathew J, Kshirsagar R, Zabeen S, Smyth N, Kanarachos S, Langer K, Fitzpatrick ME (2021) Machine learning-based prediction and optimisation system for laser shock peening. Appl Sci 11:2888. https://doi.org/10.3390/app11072888
19. Miao HY, Larose S, Perron C, Lévesque M (2010) An analytical approach to relate shot peening parameters to Almen intensity. Surf Coat Technol 205:2055–2066. https://doi.org/10.1016/j.surfcoat.2010.08.105
20. Wu J, Li Y, Zhao J, Qiao H, Lu Y, Sun B, Hu X, Yang Y (2021) Prediction of residual stress induced by laser shock processing based on artificial neural networks for FGH4095 superalloy. Mater Lett 286:129269. https://doi.org/10.1016/j.matlet.2020.129269
21. Wu J, Liu X, Qiao H, Zhao Y, Hu X, Yang Y, Zhao J (2021) Using an artificial neural network to predict the residual stress induced by laser shock processing. Appl Opt 60:3114–3121. https://doi.org/10.1364/AO.421431
22. Atig A, Ben Sghaier R, Seddik R, Fathallah R (2018) Probabilistic methodology for predicting the dispersionof residual stresses and Almen intensity considering shot peening process uncertainties. Int J Adv Manuf Technol 94:2125–2136. https://doi.org/10.1007/s00170-017-1033-3
23. Prevéy PS (1990) X-ray diffraction characterization of residual stresses produced by shot peening. In: Niku-Lari A (ed) Shot peening theory and application, IITT International, Gournay-Sur-Marne, France, pp 81–93
24. Xie L, Zhang J, Xiong C, Wu L, Jiang C, Lu W (2012) Investigation on experiments and numerical modelling of the residual stress distribution in deformed surface layer of Ti–6Al–4V after shot peening. Mater Des 41:314–318. https://doi.org/10.1016/j.matdes.2012.05.024

25. Al-Obaid YF (1995) Shot peening mechanics: experimental and theoretical analysis. Mech Mater 19:251–260. https://doi.org/10.1016/0167-6636(94)00036-G
26. Zhang JY, Yao CF, Cui MC, Tan L, Sun YQ (2021) Three-dimensional modeling and reconstructive change of residual stress during machining process of milling, polishing, heat treatment, vibratory finishing, and shot peening of fan blade. Adv Manuf 9:430–445. https://doi.org/10.1007/s40436-021-00351-4
27. Tan L, Zhang D, Yao C, Wu D, Zhang J (2017) Evolution and empirical modeling of compressive residual stress profile after milling, polishing and shot peening for TC17 alloy. J Manuf Process 26:155–165. https://doi.org/10.1016/j.jmapro.2017.02.002
28. Li JK, Mei Y, Duo W, Renzhi W (1991) Mechanical approach to the residual stress field induced by shot peening. Mater Sci Eng, A 147:167–173. https://doi.org/10.1016/0921-5093(91)90843-C
29. Barber JR, Ciavarella M (2000) Contact mechanics. Int J Solids Struct 37:29–43. https://doi.org/10.1016/S0020-7683(99)00075-X
30. Yao C, Zhang J, Cui M, Tan L, Shen X (2020) Machining deformation prediction of large fan blades based on loading uneven residual stress. Int J Adv Manuf Technol 107:4345–4356. https://doi.org/10.1007/s00170-020-05316-8
31. Wu LH, Jiang CH (2017) Effect of shot peening on residual stress and microstructure in the deformed layer of Inconel 625. Mater Trans 58:164–166. https://doi.org/10.2320/matertrans.M2016298
32. Wu L, Jiang C (2019) Investigation on surface layers characteristics of pre-stressed shot peening Inconel 625. Mater Trans 60:2558–2561. https://doi.org/10.2320/matertrans.MT-M2019106
33. Chen M, Liu H, Wang L, Wang C, Zhu K, Zhou Xu, Jiang C, Ji V (2018) Evaluation of the residual stress and microstructure character in SAF 2507 duplex stainless steel after multiple shot peening process. Surf Coat Technol 344:132–140. https://doi.org/10.1016/j.surfcoat.2018.03.012
34. Asgari A, Dehestani P, Poruraminaie I (2017) On the residual stress modeling of shot-peened AISI 4340 steel: finite element and response surface methods. Mech Ind 18:605. https://doi.org/10.1051/meca/2017033
35. Ohta T, Ma N (2020) Shot velocity measurement using particle image velocimetry and a numerical analysis of the residual stress in fine particle shot peening. J Manuf Process 58:1138–1149. https://doi.org/10.1016/j.jmapro.2020.08.059
36. Wang X, Wang Z, Gang Wu, Gan J, Yang Y, Huang H, He J, Zhong H (2019) Combining the finite element method and response surface methodology for optimization of shot peening parameters. Int J Fatigue 129:105231. https://doi.org/10.1016/j.ijfatigue.2019.105231
37. Wang T, Platts MJ, Levers A (2006) A process model for shot peen forming. J Mater Process Technol 172:159–162. https://doi.org/10.1016/j.jmatprotec.2005.09.006
38. Levers A, Prior A (1998) Finite element analysis of shot peening. J Mater Process Technol 80–81:304–308. https://doi.org/10.1016/S0924-0136(98)00188-5
39. Grasty LV, Andrew C (1996) Shot peen forming sheet metal: finite element prediction of deformed shape. Proc Inst Mech Eng, Part B: J Eng Manuf 210:361–366. https://doi.org/10.1243/PIME_PROC_1996_210_129_02
40. Zhan C (2016) A high efficient surface-based method for predicting part distortions in machining and shot peening. Int J Mech Sci 119:125–143. https://doi.org/10.1016/j.ijmecsci.2016.09.032
41. Zhang J, Yao C, Tan L, Cui M, Lin Z, Han W, Min X (2021) Shot peening parameters optimization based on residual stress-induced deformation of large fan blades. Thin-Walled Struct 161:107467. https://doi.org/10.1016/j.tws.2021.107467
42. Skinner RD (1978) Stress-peen straightening of complex machined aircraft parts. Formability Topics-Met Mater. https://doi.org/10.1520/STP30048S
43. He Y, Wang D, Wang Y, Zhang H (2016) Correction of buckling distortion by ultrasonic shot peening treatment for 5A06 aluminum alloy welded structure. Trans Nonferrous Metals Soc China 26:1531–1537. https://doi.org/10.1016/S1003-6326(16)64259-0
44. Miao HY, Lévesque M, Gosselin FP (2022) Shot peen forming pattern optimization to achieve cylindrical and saddle target shapes: the inverse problem. CIRP J Manuf Sci Technol 36:67–77. https://doi.org/10.1016/j.cirpj.2021.11.003
45. Zhang Z, Luo M, Tang K, Zhang D (2020) A new in-processes active control method for reducing the residual stresses induced deformation of thin-walled parts. J Manuf Process 59:316–325. https://doi.org/10.1016/j.jmapro.2020.09.079
46. Li X, Li L, Yang Y, Zhao G, He N, Ding X, Shi Y, Fan L, Lan H, Jamil M (2020) Machining deformation of single-sided component based on finishing allowance optimization. Chin J Aeronaut 33:2434–2444. https://doi.org/10.1016/j.cja.2019.09.015
47. Chu GC, Hu FZ, Jin XJ, Zhang Y, Wang Q, Hou JP, Zhang ZF (2022) Fatigue properties improvement of low-carbon alloy axle steel by induction hardening and shot peening: a prospective comparison. Acta Metall Sin (Engl Lett). https://doi.org/10.1007/s40195-021-01366-3